

See discussions, stats, and author profiles for this publication at: <https://www.researchgate.net/publication/263949905>

Multiobjective Optimization of Cold-End Separation Process in an Ethylene Plant

ARTICLE *in* INDUSTRIAL & ENGINEERING CHEMISTRY RESEARCH · NOVEMBER 2013

Impact Factor: 2.59 · DOI: 10.1021/ie4027764

CITATIONS

2

READS

98

2 AUTHORS:



[Shruti Pandey](#)

National University of Singapore

1 PUBLICATION 2 CITATIONS

[SEE PROFILE](#)



[Gade Pandu Rangaiah](#)

National University of Singapore

240 PUBLICATIONS 2,389 CITATIONS

[SEE PROFILE](#)

Multiobjective Optimization of Cold-End Separation Process in an Ethylene Plant

Shruti Pandey and G. P. Rangaiah*

Department of Chemical and Biomolecular Engineering, National University of Singapore, Engineering Drive 4, Singapore 117585

ABSTRACT: Ethylene and propylene separation from the mixture produced by steam cracking of saturated hydrocarbons is a highly energy-intensive process. In this, plant operators face several problems due to changes in feedstock, loss of ethylene and propylene with other streams in intermediate columns, varying demand for ethylene and propylene, and higher utility consumption. Plants need to adjust the operating conditions to maximize profit while meeting the product demand and specifications. In order to maximize profit, it is important to reduce losses as well as energy requirements, which are conflicting and require multiobjective optimization (MOO). In this study, cold-end separation process of an ethylene plant is simulated in Aspen Hysys, and the simulation model is validated with typical design data. Then, using this model, MOO of the cold-end separation system is studied using the elitist nondominated sorting genetic algorithm. It is shown that the plant can be operated at different optimal conditions, each of which involves some trade-off among the objectives of interest.

1. INTRODUCTION

Ethylene is a key building block in the petrochemical industry. The majority of ethylene is used in the production of ethylene oxide, ethylene dichloride, ethyl benzene, and a variety of homo- and copolymers (i.e., plastics ranging from food wrap to impact-absorbing dashboards in cars). Increasing modernization and urbanization in developing countries in Asia have created new markets for these products, thereby accelerating the demand for ethylene. This has resulted in large capacity expansions in recent years, with capacity growing at an annual growth rate of 4% from 2007 to reach 155.9 million tonnes of ethylene/annum in 2012.¹ Ethylene plants are complex, large-scale factories that can process a variety of feedstock ranging from gases (such as ethane, propane, and liquefied petroleum gas) to naphtha, distillates, and gas oils. Local market and extent of integration of ethylene units into refining and/or petrochemical complexes influence the products desired and the feedstocks used. The main products are polymer-grade ethylene and propylene, and others such as butadiene-rich C4 stream and C6–C8 aromatics-rich pyrolysis gasoline.

The ethylene production process has been the subject of research for a long time. Many studies have been reported on analyzing this process, optimizing the process flow-sheet, and suggesting modifications.^{2–6} These studies have helped to gain better insight into the process and to identify the scope for modifications at both design and operation stages. However, they mainly examine ethylene plants from pyrolysis furnaces to demethanizer, and by single objective optimization. The separation train after demethanizer was not considered in these studies.

The separation train in the cold-end of the ethylene plant comprises many distillation columns, which separate reactor effluent into valuable products like ethylene and propylene, and also recover ethane and propane for possible recycling. Various attempts have been made to modify and optimize this separation section. Sobočan and Glavić⁷ performed optimization of two best sequences of distillation columns for a six-product separation, including a case study on ethylene process.

Wang and Smith⁸ focused on synthesis and optimization of specialized sequences including flash drums, dephlegmators, and simple and complex distillation columns to minimize total shaft power requirement of the refrigeration system or total utility costs. Van Geem and Marin⁹ studied the design of an ethylene separation process using advanced computational methods and found the best configuration out of demethanizer-first, deethanizer-first, and depropanizer-first process design in combination with front-end or back-end hydrogenation. The operation optimization of cold-end separation process of an ethylene plant was also studied by some groups. Zhang et al.¹⁰ modeled the chilling train before demethanizer and then optimized it using GAMS software. Tahouni et al.¹¹ studied operation optimization of low-temperature separation in an olefin plant. They analyzed retrofitting of separation columns, which involved reflux ratio optimization, feed conditioning and side condensing, and reboiling. In another study, Tahouni et al.¹² modified the basic design procedure for the cold-end separation system and its associated refrigeration cycles, to determine appropriate and cost-effective separation schemes along with integrated refrigeration systems.

It is evident from the above review that multiobjective optimization (MOO) of the cold-end separation process of an ethylene plant has not been explored so far. The objectives considered in the above cases may be conflicting and affect the process optimization in opposite directions. Hence, it is important to understand the nature of conflict between different objectives. MOO provides a set of optimal solutions in the form of a Pareto-optimal front, where moving from one solution to another involves some trade-off in at least one objective. It has been applied to various chemical processes in

Received: August 23, 2013

Revised: October 25, 2013

Accepted: November 5, 2013

Published: November 5, 2013



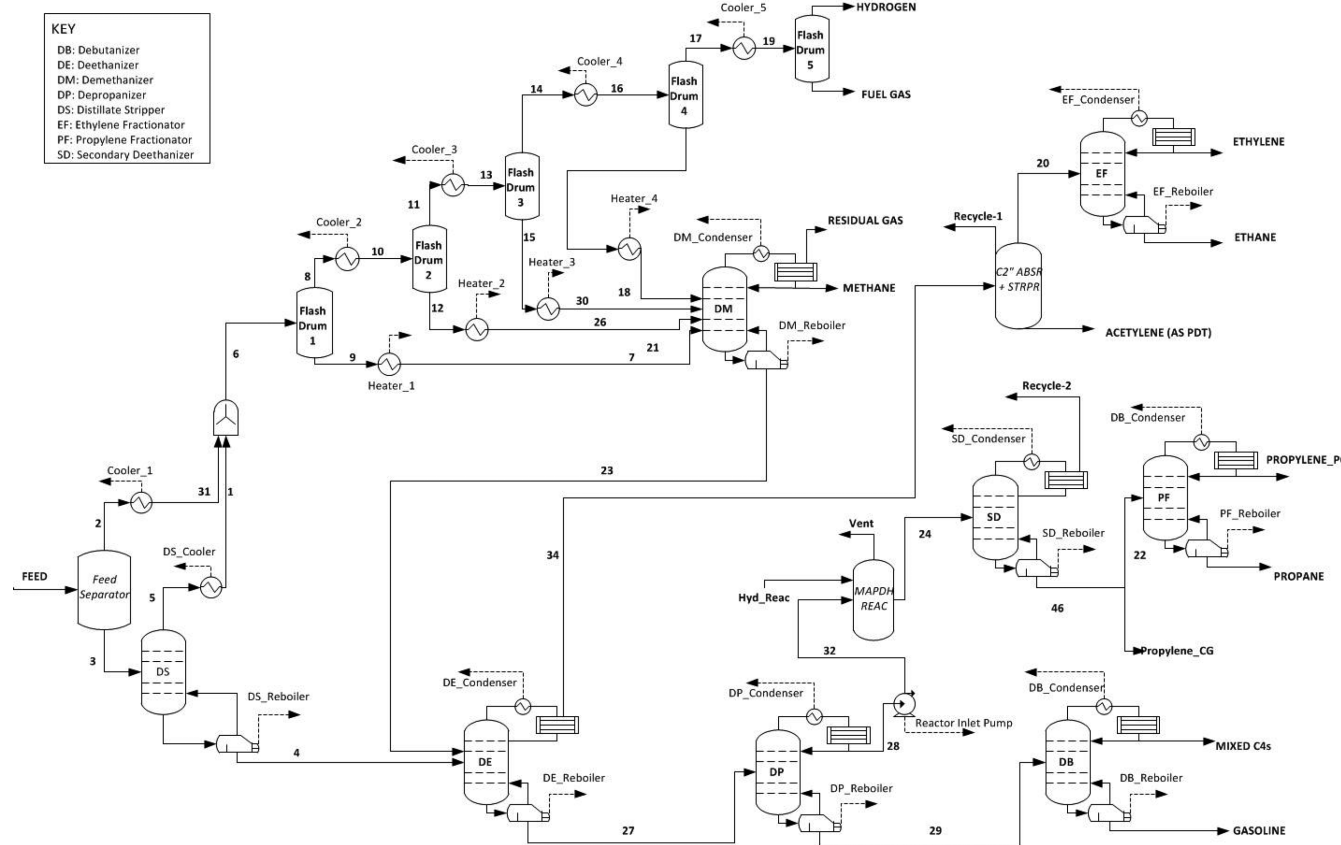


Figure 1. Process flow diagram of the cold-end separation system of an ethylene plant.

recent years.^{13,14} However, MOO studies on the ethylene process are limited to naphtha cracker only.^{15–19}

In the present study, the cold-end separation section of ethylene production, which comes after the pyrolysis and compression sections, is analyzed and optimized for multiple objectives. This study considers a train of distillation columns, intercepted by a methyl-acetylene propadiene hydrogenation (MAPDH) reactor and an acetylene recovery section, to produce ethylene, propylene, acetylene, ethane, propane, C4's, and gasoline. The elitist nondominated sorting genetic algorithm NSGA-II is employed for MOO. Several biobjective cases involving important and conflicting objectives are considered for MOO of the cold-end separation process. The results on the trade-off between objectives and optimal values of decision variables are presented and discussed for deeper insight into the process. The rest of this paper is organized as follows. Section 2 describes the ethylene production process. Section 3 presents the simulation and validation of the cold-end separation process adopted for this study. Section 4 covers formulation of MOO problems, which includes selection of objectives, decision variables, and constraints in the optimization problems solved. In section 5, results from the optimization of several combinations of two objectives are presented and discussed. Finally, conclusions of this study are given in section 6.

2. PROCESS DESCRIPTION

In a typical ethylene plant, hydrocarbons along with superheated steam, at radiant-coil inlet temperature of about 600 °C, are sent to the tubular reactor for pyrolysis. Cracked gases leave the radiant coil of an ethylene furnace at 750–900 °C.

Thereafter, the effluent is quickly cooled in exchangers by generating steam. Quench oil is directly sprayed into the cracker effluent which reduces the temperature quickly, in order to minimize further cracking into undesired products. This is followed by a gasoline fractionator to recover fuel oil and lighter components from the heavies in the cracked effluent. The top product of the gasoline fractionator is sent to a quench tower to condense all the steam and most of the pyrolysis gasoline components. A series of 3–4 compressor stages is used to increase the pressure of the quench tower exit stream to ~1.5 MPa. After an acid gas removal system, another stage of compression up to 3.5 MPa and cooling by propylene refrigerant to slightly above hydrate formation temperature, the stream is flashed into vapor and condensate. This flash vessel is the starting point of the cold section of an ethylene plant (i.e., cold-end separation process).

The separation process studied in this work is shown in Figure 1. In this process, the vapor from the flash vessel, Feed_Separator, comprising C₂ and lighter components goes through stage-wise condensation using propylene–ethylene cascade refrigeration, also known as the chilling box, to finally separate hydrogen and fuel gas in Flashdrum_5. The condensates from Flashdrum_1, Flashdrum_2, Flashdrum_3, and Flashdrum_4 are directed to appropriate trays in the demethanizer, DM, as feed streams. DM's overhead vapor stream, RESIDUAL GAS, comprises 95 mol % methane, and the rest is H₂ and CO with traces of ethylene; the distillate stream, METHANE, has traces of hydrogen and ethylene. DM's bottoms stream contains primarily C₂ and heavier products.

The condensate from the Feed_Separator is fed into the distillate stripper, DS, whose overhead stream containing lighter hydrocarbons up to C4's is sent to the chilling box, along with the vapor from the flash vessel, Feed_Separator. The bottoms from both DS and DM are supplied to the deethanizer, DE, operating at ~ 2.6 MPa. The overhead stream of DE is mainly C2's, namely, ethylene, ethane, and acetylene, and the bottom stream contains C3's and higher. The acetylene in DE overheads is recovered using extractive distillation by passing through several absorption-desorption towers, represented together as C2" ABSR + STRPR in Figure 1.²⁰ In the first tower, acetylene along with some ethylene and ethane is absorbed in dimethylformamide. The second tower recovers the absorbed ethylene and ethane, and the third tower desorbs acetylene into the outlet stream. After the acetylene is recovered, the gas is sent to the ethylene fractionator, EF, which is an ethylene–ethane separator typically producing 99.9 mol % ethylene in overheads and more than 99 mol % ethane in bottoms. Ethane is recycled to tubular heaters for steam cracking into valuable products.

The DE bottoms are fed to the depropanizer, DP, whose overhead stream is C3 hydrocarbons including propylene, propane, methylacetylene, and propadiene. This stream is sent to the hydro-converter, MAPDH_REAC, with catalysts that convert methyl-acetylene and propadiene to propene and propane.²⁰ The hydrogenated stream is sent to the secondary deethanizer, SD, whose vent is recycled. Bottoms of SD are supplied to the propylene fractionator, PF, operating at 1.8–2 MPa and having more than 200 trays in two-tower design. PF produces polymer-grade propylene (99.5%+) in the overheads and propane with purity of more than 95% in the bottoms. The latter can either be recycled to the steam cracker or used as a fuel. DP's bottoms with C4 and heavier hydrocarbons is fed into the debutanizer, DB, operating at 0.4–0.5 MPa; DB produces distillate comprising mainly C4's and bottoms having C5's and higher.

The separation system shown in Figure 1 has demethanizer in the beginning and hydrogenation reactor toward the end. Other separation schemes (e.g., deethanizer first or depropanizer first with front-end or back-end hydrogenation) are possible.⁹ The scheme shown in Figure 1 is chosen for the present study as its typical design data are available from our source, who wishes to remain anonymous.

3. SIMULATION OF THE COLD-END SEPARATION PROCESS

The cold-end separation section of the existing plant comprises 8 distillation columns, 6 flash drums, 6 coolers, 4 heaters, and a reactor (Figure 1), and it is simulated using Aspen HYSYS version 7.2. The simulation procedure involves selection of a property package, which estimates thermodynamic and transport properties for the multicomponent mixtures in the process. Two important tasks to ensure accurate estimation of physical properties for simulation are selecting the appropriate physical property method(s), and validating the physical properties predicted.²¹ Preliminary selection of property methods requires consideration of the following: (a) nature of properties of interest, (b) composition of the mixture, (c) pressure and temperature ranges, and (d) availability of parameters in the property model. On the basis of these considerations, two property models, Soave–Redlich–Kwong (SRK) and Peng–Robinson (PR) model catering to real and nonpolar components, were selected for further deliberation.

Extensive vapor–liquid equilibrium (VLE) validation was done to choose one of these models by simulating the experimental VLE data available in Gmehling et al.²² In total, seven binary VLE data for key components in the distillation columns involved were considered. Adjusted R^2 values between experimental and simulated VLE data showed that predictions by PR model fitted the experimental data better than those by SRK model; therefore, the former was selected as the property package for simulating the cold-end separation process of the ethylene plant.

3.1. Details of the Process and Simulation. The cold-end separation process used in this study is based on a simplified and yet realistic process flow diagram, typical of plants built in the early 1980s using naphtha as the feedstock. The feed for the separation process is a mixture of gases, leaving the multistage compression and caustic wash section. It comprises hydrogen, methane, C2's, C3's, C4's, C5's, and C6's, with typical composition shown in Table 1; this feed composition was obtained from our anonymous source. The C7's and higher components were combined together with C6's, and they are all considered as n-hexane.

Table 1. Feed Composition for the Cold-End Separation Process

component	mole fraction
hydrogen, H ₂	0.1445
methane, CH ₄	0.2627
acetylene, C ₂ H ₂	0.0056
ethylene, C ₂ H ₄	0.3172
ethane, C ₂ H ₆	0.0608
methyl-acetylene, C ₃ H ₄	0.0023
propadiene, C ₃ H ₄	0.0023
propene, C ₃ H ₆	0.1135
propane, C ₃ H ₈	0.0053
butadienes, C ₄ H ₆	0.0252
butenes, C ₄ H ₈	0.0120
butanes, C ₄ H ₁₀	0.0168
n-pentane, C ₅ H ₁₂	0.0155
n-hexane, C ₆ H ₁₄	0.0150
carbon monoxide, CO	0.0012

The distillation columns are simulated rigorously via stage-by-stage calculations. The operating pressure and number of trays are typical of an operating plant. Column bottom pressure was estimated assuming 0.1 psi pressure drop per tray. By knowing the actual number of trays in each column, the number of ideal trays can be estimated using overall efficiency of the column from the O'Connell correlation:²³

$$E_0 = 51 - 32.5 \log(\mu_a \alpha_a) \quad (1)$$

This efficiency is based on feed liquid viscosity (μ) and the relative volatility of light-heavy key components (α_{LK-HK}) at the column average conditions. Overall efficiency thus calculated for each column is consistent with the ranges given in the literature (Table 2). On the basis of calculated efficiencies, the number of ideal trays was calculated as follows:

number of ideal trays

$$= \text{actual number of trays} \times \text{overall efficiency} \quad (2)$$

In Aspen HYSYS, stage/tray efficiency can be given for simulating columns. The column model is probably based on

Table 2. Key Components and Overall Efficiency for Columns in the Cold-End Separation Process Shown in Figure 1

distillation column ^a	overall efficiency (%)		
	calcd	Kaes ²⁴	GPSA ²⁵
DS (methane, n-butane)	43	40–50	
DM (methane, propane)	72		45–60
DE (ethane, propene)	79	65–70	60–75
DP (propene, i-butene)	72	70–80	80–90
DB (propane, n-butane)	73	85–90	85–95
SD (ethane, propane)	84	65–70	
PF (propylene, propane)	95	95–100	
EF (ethylene, ethane)	87	95–100	

^aWith light and heavy keys in parentheses.

equilibrium stages, and stage efficiency is used to correct compositions of liquid and vapor streams leaving a stage. This, according to Kaes,²⁴ makes the column model inappropriate for prediction at other operating conditions, if stage efficiencies are used. It was suggested to use overall efficiency to translate the actual trays to ideal trays, and then simulate the column with ideal trays. Hence, the number of ideal trays calculated as above using the overall efficiency was used in the HYSYS simulation of distillation columns. The feed stage for each column was changed according to its overall efficiency.

Various configurations were used for different columns depending upon their reflux conditions in the plant. DM has a partial condenser, and hence its simulation requires 3 active specifications, which are overhead vapor flow rate, distillate flow rate, and reflux ratio. DE and SD use full reflux conditions (i.e., with only a vapor stream as the distillate), and so vent rate and reflux rate are used as active specifications for their simulation. DP and DB use total condenser, and are simulated with specified distillate rate and reflux ratio. For the EF and PF, total condensers are used. Since these produce final products, active specifications for their simulation are the product compositions as given in the design data.

In the present study, major heat-integrated networks inside chilling-box before DM are not considered for simplicity. Data on the acetylene recovery section are not available due to proprietary reasons, and so it is replaced by a component splitter for simulation purpose. The MAPDH_REAC is simulated as a conversion reactor along with a component splitter to closely simulate this complex reactor system. A few streams are returned to the upstream section of the plant (i.e., steam cracker), and so they are considered as such without any recycle (block) in the HYSYS simulation.

3.2. Validation of the Simulation. For validating the predictions by Aspen HYSYS, all the units in the process shown in Figure 3 were simulated on the basis of the design data of a typical operating plant outlined in the previous section. The product specifications were followed as per the design data as well. The solver used for all distillation columns was HYSIM inside-out algorithm except for DM which required the modified HYSIM inside-out for robust convergence. The component splitters for simulating the acetylene recovery section and MAPDH_REAC section have been assigned split values according to the design data. Predicted stream conditions are compared with the typical design data in Table 3. For each distillation column, absolute error is calculated in case of temperatures, and both absolute and

Table 3. Comparison of Predicted Flow Rates with the Typical Design Data

distillation column	output stream	design value (kg/h)	predicted value (kg/h)	absolute error (%)
Feed_Separator	overheads	84 788	86 386	1598 (1.9%)
	bottom	36 018	34 420	1598 (4.4%)
DS	bottoms	28 317	26 720	1597 (5.6%)
DM	bottoms	71 382	73 036	1654 (2.3%)
DE	bottoms	49 339	49 396	57 (0.1%)
DP	bottoms	25 113	25 170	57 (0.2%)
DB	bottoms	11 175	11 232	57 (0.5%)
SD	bottoms	24 247	24 241	6 (0.0%)
EF	overheads	39 830	39 780	50 (0.1%)
	bottoms	8227	8269	42 (0.5%)
PF	overheads	15 312	15 308	4 (0.0%)
	bottoms	1083	1084	1 (0.1%)

percentage errors are given for the overhead and bottoms flow rates.

Referring to the first three entries in Table 3, the difference in the predicted bottoms flow rate of DS from the design data is due to lesser amount of liquid from Feed_Separator flowing into DS as top stage feed. This may be due to the property package used in the simulation which affects the flash calculations of Feed_Separator. However, it is recovered back through the DM which is supplied with the vapor stream from Feed_Separator.

Interestingly, DM bottoms flow rate error is 57 kg/h higher than DS bottoms flow rate error in the simulation (Table 3). This accounts for the extra 57 kg/h of components coming into the DE from the DM bottoms, which were supposed to go out through HYDROGEN and FUEL GAS, as per the design data. Since DE vent rate was fixed according to the design data as an active specification for the column, the predicted flow rate of DE bottoms is 57 kg/h higher than the design value since more of the propene and ethane are driven to the bottoms. Similarly, distillate rate is specified for DP. Hence, extra propene entering the column is sent through overheads instead of some methyl-acetylene, butadienes, and other C4's which go to the DP bottoms. Small errors in product flow rates of EF are partly attributed to the physical property model and partly to the lesser amount of propene (22 kg/h) entering the column.

Results in Table 4 show that DS overheads temperature is predicted to be 6.8 °C lower than the design value. This may be because of the differences in the physical property model used for this column in the present simulation and in that used for the typical design. Predicted temperatures of DP and DB bottoms are 4 and 11.5 °C higher than the design data due to more heavies going to DP and DB bottoms, relative to the design data. In general, most of the errors are small, and the Aspen HYSYS simulation model can be used for optimization.

4. FORMULATION OF MULTIOBJECTIVE OPTIMIZATION PROBLEMS

In large-scale processes like the cold-end separation system under consideration, there are many factors which play a crucial role in the selection of objective functions. It is therefore important to study different objectives separately as well as together in right combinations to draw meaningful conclusions.

Table 4. Comparison of Predicted Temperatures with the Typical Design Data

distillation unit-output stream	design value (°C)	predicted value (°C)	absolute error
DS-overheads	36.7	29.9	6.8
DS-bottoms	101.3	102.2	0.9
DM-overheads	-96.3	-97.9	1.6
DM-bottoms	6.9	6.0	0.9
DE-overheads	-16.1	-15.9	0.2
DE-bottoms	87.6	88.5	0.9
DP-overheads	-1.1	-0.4	0.7
DP-bottoms	67	71.0	4
DB-overheads	37.8	39.3	1.5
DB-bottoms	95	106.4	11.5
SD-overheads	37.8	37.8	0.0
SD-bottoms	51.9	52.2	0.3
EF-overheads	-28.9	-29.0	0.1
EF-bottoms	-5.7	-5.8	0.1
PF-overheads	43.4	43.8	0.4
PF-bottoms	55.6	53.9	1.7

Often, optimization is carried out to minimize the most common objective, namely, profit. Since profit is the difference of revenue and cost, reducing cost and/or increasing revenue drive(s) the profit upward. In the present case study, the prime source of revenue is from ethylene and propylene production. Hence, they are selected as two objectives to be maximized. The counteracting factor for each of them is the net utility cost of distillation columns, which increases with production rate. So, it is important to minimize the net utility cost, which accounts for both cost of total utilities consumed and utility credits. There are two sources of credit for cold energy produced in the separation process: (a) utility used in DM reboiler is chilled water leaving at about 5 °C, and (b) utility used in EF reboiler is propylene leaving at about -2 °C. These give rise to another objective function in the form of maximizing utility credit obtained from the plant. See Table 5 for the utility data and prices used in the present study.

Table 5. Utility Data and Prices Used in the Study^a

utility	temperature	unit price
refrigerant (ethylene)	-101 °C	21 \$/GJ
refrigerant (propylene)	-35 °C	10.6 \$/GJ
refrigerant (propylene)	-20 °C	8.2 \$/GJ
refrigerant (propylene)	-2 °C	5.4 \$/GJ
chilled water	5 °C	4.4 \$/GJ
low pressure steam (1.03 barg)	120 °C	29.3 \$/t
cooling water	30 °C	0.0148 \$/m ³

^aValues for the refrigerants and chilled water are based on the data in Seider et al.²⁶ and those for low pressure steam and cooling water are from Turton et al.²⁷

For meaningful MOO, we need to couple the chosen objectives in a way that they are conflicting in nature. Hence, the following sets of two objectives are considered for MOO: (case 1) maximization of ethylene production and minimization of net utility cost, (case 2) maximization of propylene production and minimization of net utility cost, and (case 3) maximization of utility credit and minimization of total utility cost.

The equations for total/net utility cost and utility credit are the following:

$$\text{total utility cost, } U$$

$$\begin{aligned} &= \Sigma(\text{reboiler utility cost for DE, DP, DB, SD and PF}) \\ &\quad + \Sigma(\text{condenser utility cost for DM, DE, DP, DB, SD, EF and PF}) + \Sigma(\text{cost of utilities for all coolers and heaters}) \end{aligned}$$

$$\text{net utility cost, net } U$$

$$\begin{aligned} &= \text{total utility cost} - (\text{DM reboiler utility credit} \\ &\quad + \text{EF reboiler utility credit}) \end{aligned}$$

$$\begin{aligned} \text{utility credit, EC} &= \text{DM reboiler utility credit} \\ &\quad + \text{EF reboiler utility credit} \end{aligned}$$

Decision Variables. These are the important variables affecting the performance of distillation columns. Manipulated variables in a distillation column are often reflux ratio and reboiler duty. Reflux ratio/rate and overhead flow rate (i.e., vapor, distillate, or vent rate), which affect reboiler duty, have been considered as decision variables for the current study. These variables and their bounds are listed in Table 6. Bounds

Table 6. Decision Variables and Their Bounds for MOO of the Cold-End Separation Process^a

decision variable	lower bound	upper bound
DM reflux ratio	3	6
DM overhead vapor rate (kg/h)	13 360	13 520
DE vent rate (kg/h)	50 100	50 360
DE reflux rate (kg/h)	38 000	50 000
DP distillate rate (kg/h)	20 000	24 226
DP reflux ratio	1.27	1.57
DB distillate rate (kg/h)	12 000	14 000
DB reflux ratio	0.87	1.27
SD vent rate (kg/h)	1000	3000
SD reflux rate (kg/h)	29 000	39 000

^aDM reflux ratio and overhead vapor rate are used in cases 1 and 3, respectively.

on reflux ratios/rates have been chosen to avoid any flooding or dry trays in the columns, and those on overhead flow rate of each column have been set to ensure convergence of the simulation.

Constraints. In the industrial scenario, it is common to specify certain requirements of some intermediate streams depending on their downstream uses. Hence, these were included in the optimization problem as constraints. Composition of C4's in bottoms and heavies in overheads of DB were specified at 0.04 and 0.003 mol fraction, respectively. In addition, ethane in DE bottoms was found to be within the range 50–1070 kg/h for simultaneous convergence of EF and PF. Since these bounds cannot be specified inside the simulation, they are specified as constraints. Product specifications of ethylene and propylene were given as active specifications of EF and PF for simulation. For the optimization study, product specifications ethylene (99.9 mol %), ethane (99.5 mol %), propylene (99 mol %), and propane (95 mol %), currently followed by the industry, were used.

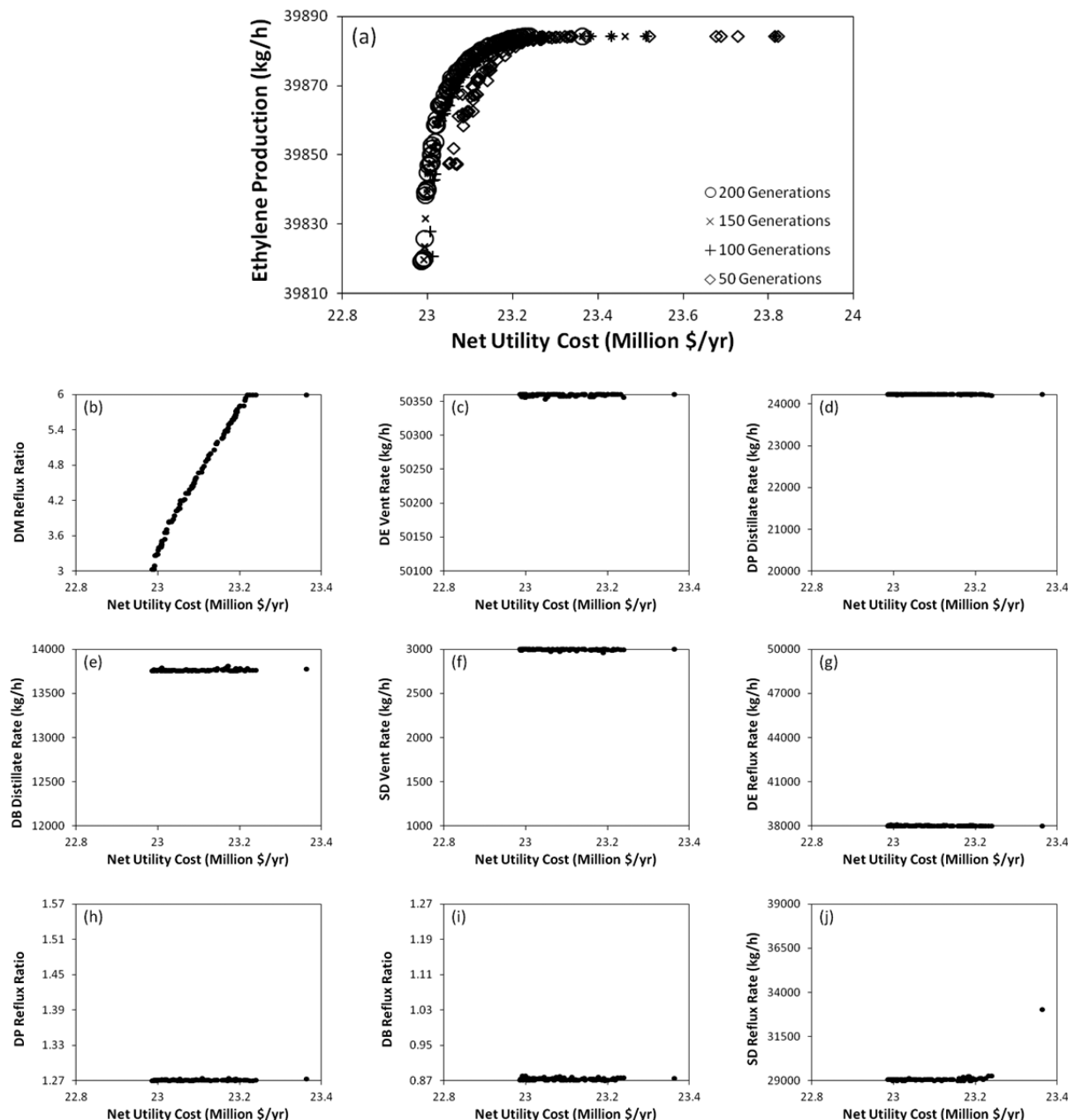


Figure 2. Pareto-optimal front for maximization of ethylene production and minimization of net utility cost at 50, 100, 150, and 200 generations (plot a); optimal values of decision variables corresponding to the Pareto-optimal front are shown in plots b–j.

Optimizer. For MOO of the cold-end separation process, the elitist nondominated sorting algorithm (NSGA-II) implemented in MS Excel using binary coding was employed.²⁸ It is called the Excel-based MOO (EMOO) program. The optimization algorithm used in this program is as follows: (1) generation of initial population of trial solutions, using uniformly distributed random numbers, within bounds of decision variables, with population size (N) set by the user; (2) send each trial solution to Aspen HYSYS through the Excel-HYSYS interface for simulating the process, which provides results, through the Excel-Hysys interface, for computing objectives to the optimizer in Microsoft Excel; (3) generation of the new population of trial solutions through genetic algorithm operations like selection, crossover, and mutation on the previous trial solutions, with step 2 repeated for each new trial solution; (4) combine the previous and current population

of trial solutions, and in this combined population, the number of individuals dominating each trial solution is found on the basis of its values of objective functions; (5) assign rank to the best Pareto front (i.e., those with no dominating individuals) as 1, and subsequent Pareto fronts as 2 onward until all trial solutions are ranked; (6) sort trial solutions on the basis of their rank, and determine the rank (ND^{cut}) of N th individual; (7) find the crowding distance in the objective space for solutions with ND^{cut} rank; (8) sort trial solutions based on increasing rank and decreasing crowding distance; (9) select the first N trial solutions in the sorted list as the current population for the next generation; (10) repeat the generation of trial solutions by the optimizer and process simulation in HYSYS (i.e., step 2 onward) for the specified maximum number of generations.

The above algorithm of EMOO program is available as a flowchart in Sharma et al.²⁹ Binary coding was employed

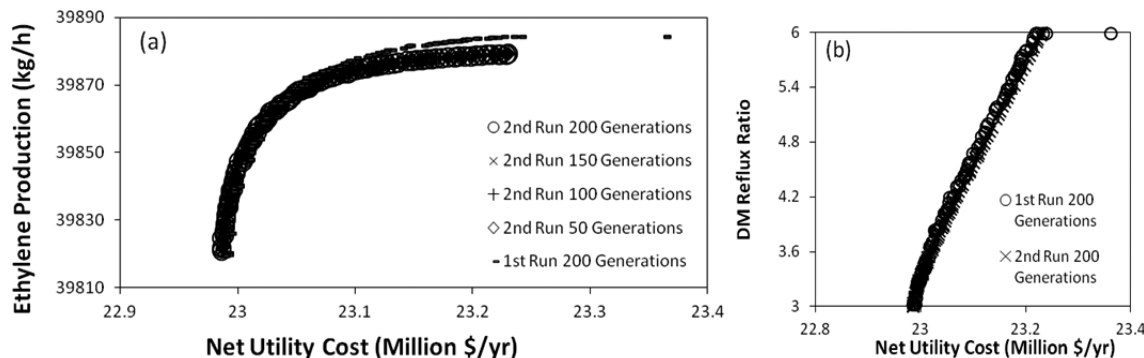


Figure 3. Pareto-optimal front for maximization of ethylene production and minimization of net utility cost with only DM reflux ratio as the decision variable and comparison of Pareto fronts obtained in the two runs are shown in plot a; optimal values of DM reflux ratio corresponding to the Pareto-optimal front for the two runs are in plot b.

because it is simple and can easily handle continuous as well as integer variables. EMOO handles inequality constraints by the constrained-dominance approach.³⁰ More details on NSGA-II and its implementation in MS Excel can be found in Sharma et al.²⁸ It has been successfully used in conjunction with process simulation in HYSYS.^{29,31,32} The optimization was performed for up to 200 generations to find the Pareto-optimal front accurately. Other algorithm parameters used in EMOO program are the following: population size = 100, two-point crossover with probability = 0.8, bit-wise mutation with probability = 0.05, tournament selection and random seed = 0.5.

5. RESULTS AND DISCUSSION

Three cases of biobjective optimization were carried out, and the obtained results are presented and discussed in this section. For each case, two optimization runs were performed: one run with all decision variables, and a second run with only a few significant decision variables based on the results of the first run; the second run was to improve/confirm the optimization results. Note that one optimization run refers to executing the algorithm given above for up to 200 generations.

5.1. Case 1: Maximization of Ethylene Production and Minimization of Net Utility Cost. Ethylene production was considered to avoid the need for the selling price of ethylene, which is subject to market demand and dynamics. Ethylene production rate depends on ethylene loss in DM, which is affected by its reflux ratio. So, only for this case, DM reflux ratio was considered as a decision variable along with others, which include vent rate and reflux rate of both DE and SD, and distillate rate and reflux ratio of both DP and DB. Net utility cost was considered on an annual basis assuming an operating time of 8760 h.

Figure 2a shows the Pareto-optimal front obtained by NSGA-II after 200 generations for maximizing ethylene production and minimizing net utility cost. The generated front shows a clear trend with reasonably well-distributed optimal solutions. As we move from one point to another toward the right of the front, ethylene production increases with increase in net utility cost. Thus, the solutions obtained after 200 generations comprise a Pareto-optimal front. Figure 2a also presents solutions at 50, 100, and 150 generations; these show that, after 100 generations, the Pareto front is nearly same with slight changes in the later part of the front. Hence, 200 generations are more than sufficient to find the Pareto-optimal front in this case. The net utility cost varied from \$23 to \$23.4

Million/year which means that an annual saving of 1.3% is possible on utility costs but at the expense of decreased ethylene production, 39 820 to 39 885 kg/h (Figure 2a). Since the ethylene production increase is steep initially, a good trade-off solution is 39 878 kg/h of ethylene production with net utility cost of \$23.1 Million/year. DM reflux ratio corresponding to this optimal solution is 4.6. All other decision variables are at their lower/upper bounds as shown in Figure 2c–j.

The optimal values of 3 decision variables DE vent rate, DP distillate rate, and SD vent rate (Figure 2c–e) are near their respective upper bound (namely, 50 360 kg/h, 24 226 kg/h, and 3000 kg/h) with DB distillate rate near its upper bound at 13 887 kg/h (Figure 2f). The feed to DE, DP, DB, and SD is in liquid phase. Higher overhead flow rates in DE, DP, DB, and SD correspond to higher reboiler and condenser duties. At the same time, they result in higher product flow rates. All the flow rates take upper bound values (and values close to upper bound for DB) since the objective of increasing ethylene production dominates the objective of decreasing utility cost. The optimal values of 4 other decision variables, DE reflux rate, DP reflux ratio, DB reflux ratio, and SD reflux rate, are near their respective lower bound, namely, 38 000 kg/h, 1.27, 0.87, and 29 000 kg/h (Figure 2g–j). This is due to the fact that when the reflux rates/ratios are low, condenser and reboiler duties are lower for fixed product purity specifications, which minimizes the objective of net utility cost.

The decision variable, affecting the two objectives in opposite directions, is DM reflux ratio. Figure 2b shows that DM reflux ratio has significant effect on ethylene production, in the beginning of the Pareto-optimal front; this corresponds to change in ethylene loss in DM condenser. This signifies the correlation between DM reflux ratio and EF distillate rate (recall that DE and the acetylene recovery section are between DM and EF). As the DM reflux ratio increases from 3 to 6, ethylene production increases by 65 kg/h. With this, duties of EF condenser and reboiler decrease slightly, but DM condenser and reboiler duties increase significantly. This leads to an increase in net utility cost. An outlier appears at the right end of the Pareto-optimal front (Figure 2a). It can be attributed to DM reflux ratio reaching its upper bound and an increase in SD reflux rate (Figure 2b,j), which increases the net utility cost but has negligible effect on ethylene production.

To confirm the Pareto-optimal solutions, another optimization run was performed with only DM reflux ratio as the decision variable while all other decision variables were set at their optimal values found in the previous run (Figure 2). The

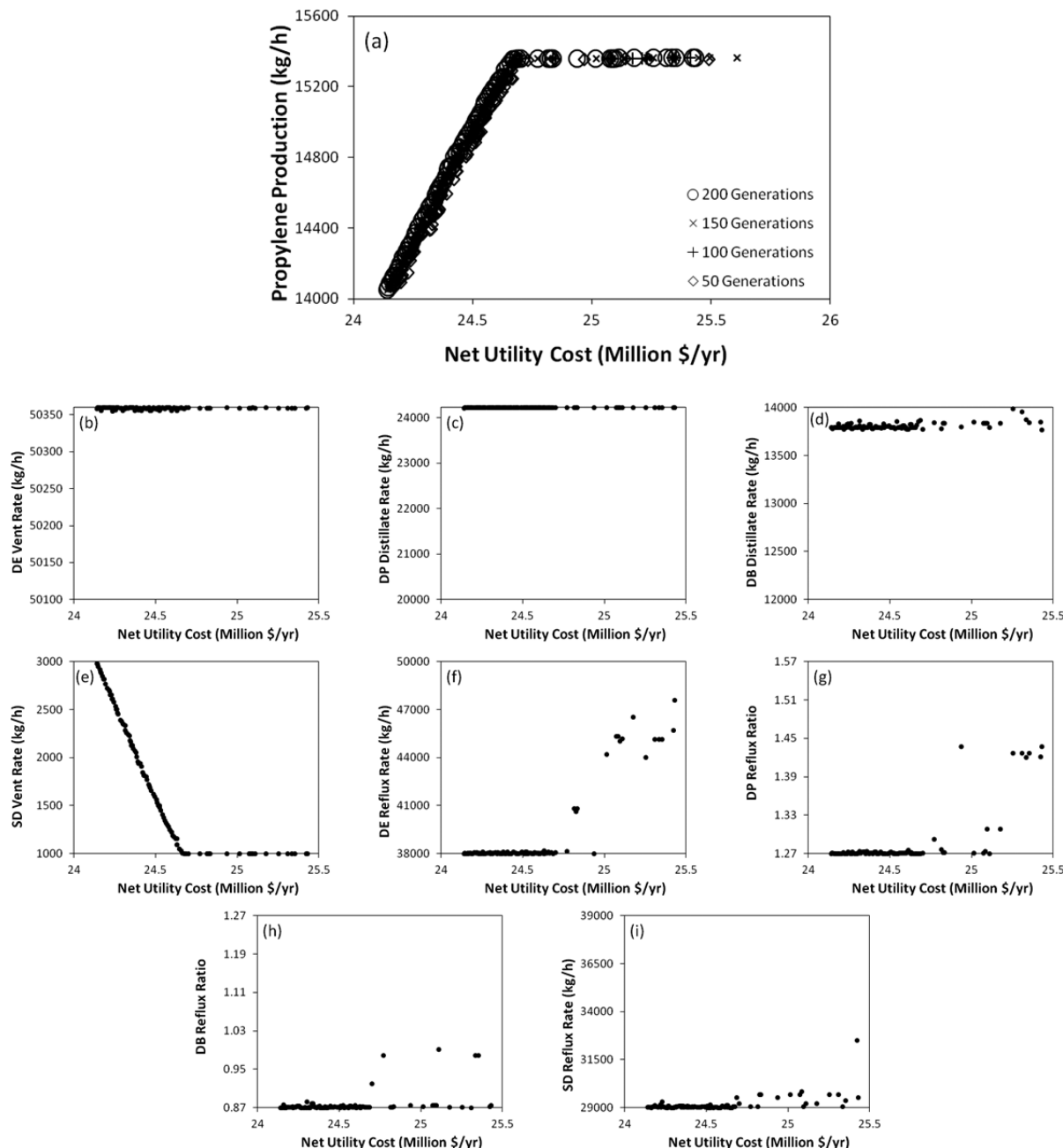


Figure 4. Optimal Pareto front for maximization of propylene production and minimization of net utility cost, at 50, 100, 150, and 200 generations (plot a); optimal values of decision variables corresponding to the Pareto-optimal front are shown in plots b–i.

obtained Pareto-optimal front is continuous and similar to that obtained in the previous run except for marginal differences at high net utility cost (Figure 3a). The outlier is no longer present, probably because SD reflux rate is no longer a decision variable. The results at a different number of generations in Figure 3a show that the Pareto-optimal front is unchanged after 50 generations. This faster convergence is expected since there is only one decision variable (Figure 3b) in the second optimization run.

5.2. Case 2: Maximization of Propylene Production and Minimization of Net Utility Cost. Hourly propylene production was maximized instead of revenue from propylene sales for the same reason as for ethylene production. As before, net utility cost was calculated on annual basis. All decision variables other than those of DM in Table 6 affect propylene

production as entire propylene input to DM goes into its bottoms. These are vent rate and reflux rate for both DE and SD, and distillate rate and reflux ratio for DP and DB. The Pareto-optimal sets obtained by NSGA-II at 50, 100, 150, and 200 generations for the maximization of propylene production and minimization of net utility cost (Figure 4a), show that, after 100 generations, the Pareto-optimal front is nearly same with slight changes in the later part of the front. Hence, 200 generations are more than sufficient to find the Pareto-optimal front in this case also. The Pareto-optimal set after 200 generations is smooth and nearly continuous in the first half of the range, and later it is nearly constant and somewhat discontinuous. The net utility cost increases by 2.1% from \$24.2 to \$24.7 Million/year as propylene production increases by 10% from nearly 14,000 to 15,400 kg/h (Figure 4a). The

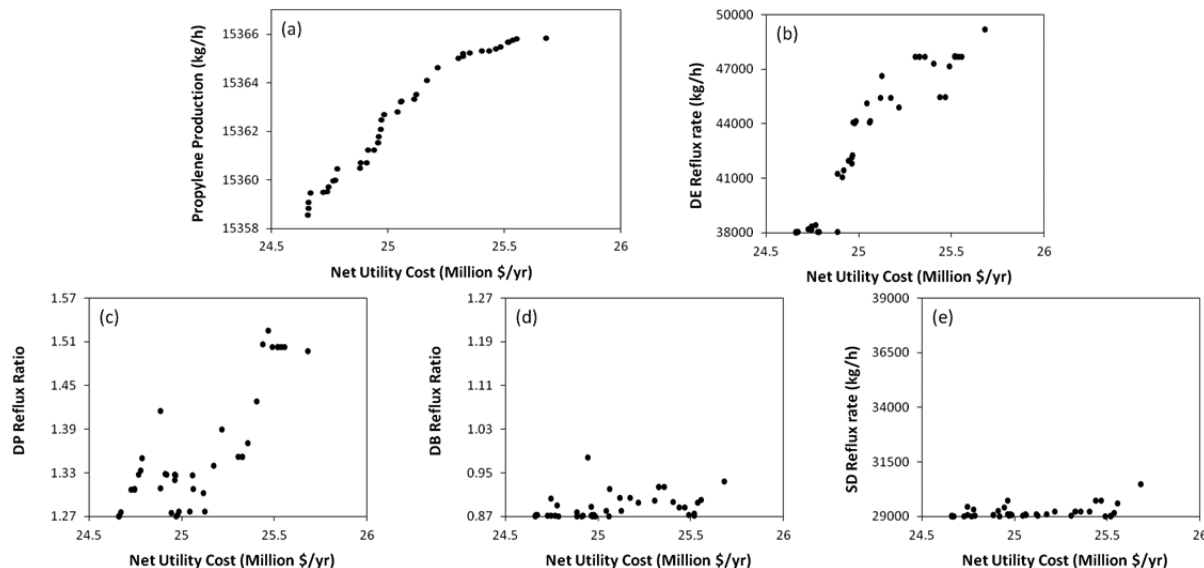


Figure 5. Optimal Pareto front for maximization of propylene production and minimization of net utility cost with reflux rates/ratios of DE, SD, DP, and DB as decision variables (plot a); optimal values of decision variables corresponding to the Pareto-optimal front are shown in plots b–e.

corner point (15 380 kg/h propylene production at utility cost of \$24.7 Million/year) in the Pareto-optimal front is the most likely choice to increase propylene production significantly with a small increase in the net utility cost. SD vent rate corresponding to this optimal solution is 3 which is its specified lower bound, and all other decision variables are at their lower/upper bound (Figure 4). When SD vent rate is the lowest possible, propylene loss from SD is the least but the reboiler utility cost is high. Since propylene loss costs more than the reboiler utility, maximizing propylene production is preferred with some trade-off in SD reboiler utility cost.

The optimal values of decision variables corresponding to the Pareto-optimal front are shown in Figure 4b–i. Optimal values of DE vent rate and DP distillate rate are at their respective upper bounds, and that of DB distillate rate is slightly away from its upper bound; these are same as in the previous case. SD vent rate is the main decision variable affecting both the objectives in the present case (Figure 4). The Pareto-optimal front (Figure 4a) shows a linear increase which is caused by a linear decrease in SD vent rate. Initially, the higher vent rate corresponds to more propylene loss, resulting in less propylene production while incurring lower net utilities cost. As the vent rate decreases, more propylene is redirected to PF, increasing propylene production. However, reboiler utility cost of SD increases pushing up the net utility cost.

The other 4 decision variables, DE reflux rate, DP reflux ratio, DB reflux ratio, and SD reflux rate, stay at their lower bounds until SD vent rate reaches its lower bound (Figure 4f–i). When SD vent rate is at its lowest bound, reflux ratios/rates of DP, DB, DE, and SD start to increase, causing propylene production to increase marginally. However, during this course, net utility cost increases substantially due to direct correlation of these decision variables with the condenser and reboiler energy requirements. To confirm this, a second optimization run was conducted with SD vent rate fixed at its lower bound, and decision variables were reflux rates/ratios of DE, SD, DP, and DB. Range of the Pareto-optimal front (Figure 5a) is limited since SD vent rate was fixed at its lower bound. The effect of decision variables in the second optimization run (Figure 5b–e) is similar to that in Figure 4. An increasing trend

of DE reflux rate and DP reflux ratio is evident; these two decision variables largely affect the net utility cost by nearly 1 million \$/year in the Pareto-optimal front. However, the increase in propylene production is insignificant (Figure 5a) since propylene production is not very dependent on reflux rates/ratios of DE, SD, DP, and DB. DB reflux ratio and SD reflux rate are mostly scattered near their respective lower bound (Figure 5d,e).

5.3. Case 3: Maximization of Utility Credit and Minimization of Total Utility Cost. Figure 6a shows the Pareto-optimal set obtained by NSGA-II after 200 generations for maximizing utility credit and minimizing total utility cost. It also presents solutions at 50, 100, and 150 generations; these show that, after 100 generations, the Pareto-optimal front is nearly the same with slight changes in the later part of the front. Hence, 200 generations are more than sufficient to find the Pareto-optimal front, which shows a neat trend with three linear segments. As we move from one point to the other toward the right, utility credit increases with increase in total utility cost. Thus, the solutions obtained after 200 generations comprise a Pareto-optimal front. The total utility cost increases by 2.1% from \$15 million/year to \$15.32 million/year as the utility credit increases by 4.5% from \$2.69 million/year to \$2.81 million/year. The most likely choice for the optimal conditions would be to operate at the starting point of the curve as the increase in utility credit is lesser than the corresponding increase in utility cost.

The optimal values of 4 decision variables, DE vent rate, DP distillate rate, DB distillate rate, and SD vent rate, are near their respective upper bounds (Figure 6c–f) whereas those of 4 other decision variables, DE reflux rate, DP reflux ratio, DB reflux ratio, and SD reflux rate, are near their respective lower bounds (Figure 6g–j). All these can be correlated to one of the objectives, i.e., minimizing total utility cost. Since utility credit comes from the DM reboiler and EF reboiler only, decision variables related to other columns take values to achieve the lowest utility cost. In this case, the decision variable causing the Pareto-optimal front is DM vent rate (Figure 6b), which affects DM reboiler duty as well as the condenser and reboiler duties of other columns.

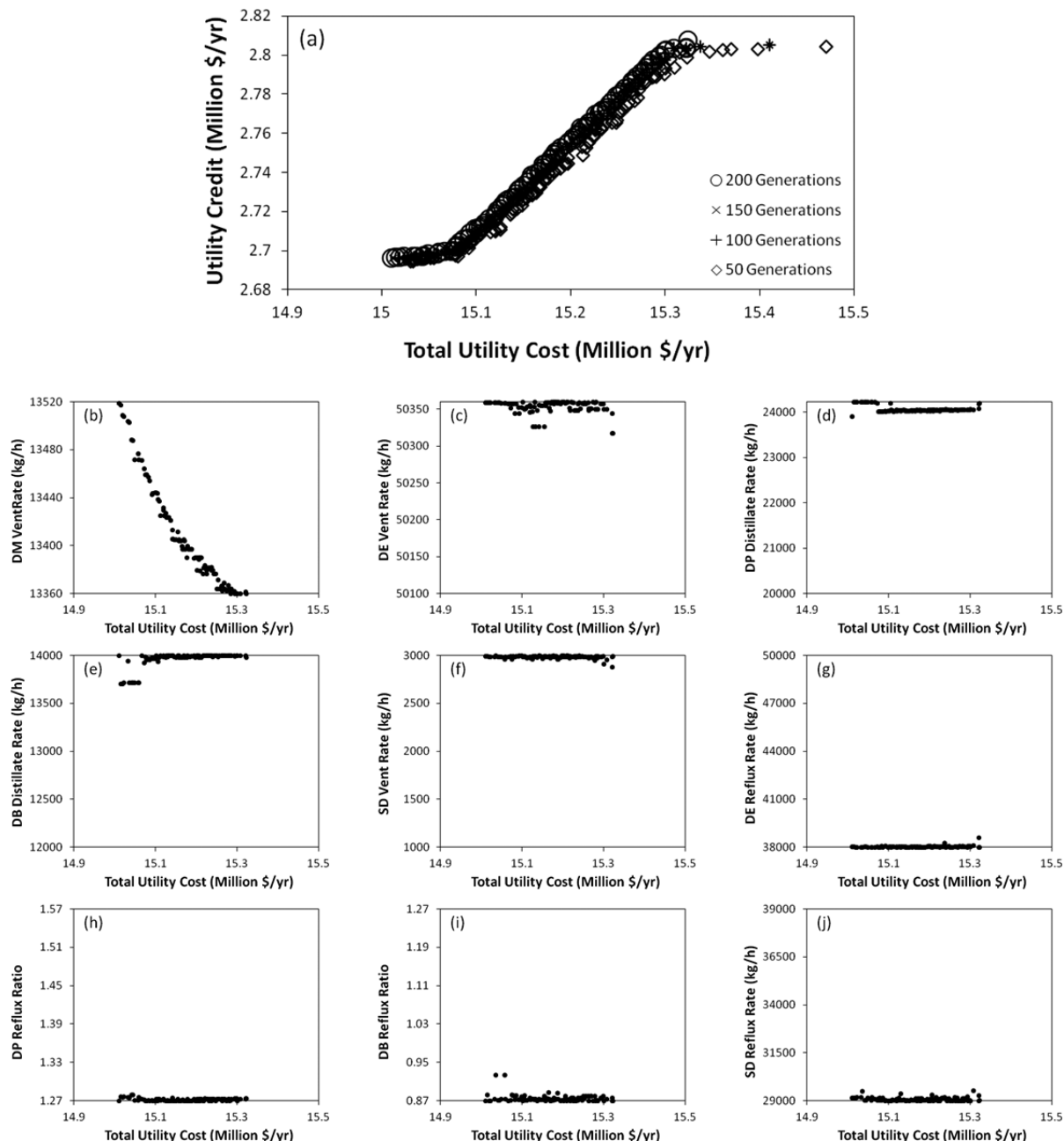


Figure 6. Optimal Pareto front for maximization of utility credit and minimization of total utility cost, at 50, 100, 150, and 200 generations (plot a); optimal values of decision variables corresponding to the Pareto-optimal front are shown in plots b–j.

The Pareto-optimal front shows a linear increase due to a nearly linear decrease in DM vent rate (Figure 6a,b). Points in the beginning of the Pareto-optimal front correspond to high vent rate, requiring lower condenser and reboiler duties for EF while generating higher reboiler utility credit from DM. As the DM vent rate decreases, condenser and reboiler utility costs of DE, SD, PF, and EF increase while the DM reboiler duty decreases. Since the utility credit is the sum of DM and EF reboiler utility credits, the slight decrease in DM reboiler utility credit is covered by major increase in EF reboiler utility credit. Hence, overall utility credit increases with decrease in DM vent rate.

The outliers generated in the 50th, 100th, and 150th generations are probably due to sudden increase in DP reflux ratio. To confirm this, second optimization run was carried out

to see the individual effect of the main decision variable, i.e., DM vent rate along with DP reflux ratio on the Pareto-optimal front. The Pareto-optimal front (Figure 7) is similar to that in the first optimization run; however, there is an outlier found at the 200th generation. Once DM vent rate reaches its lower bound, DP reflux ratio increases causing an increase in the total utility cost. However, since DP reflux ratio does not affect the reboiler duties of DM and EF, there are no significant effects on the utility credit. Nevertheless, changing the DM vent rate only, with overhead flow rates at their respective upper bounds and reflux ratios/rates at their respective lower bounds in other columns, is sufficient for obtaining the Pareto-optimal front in this case.

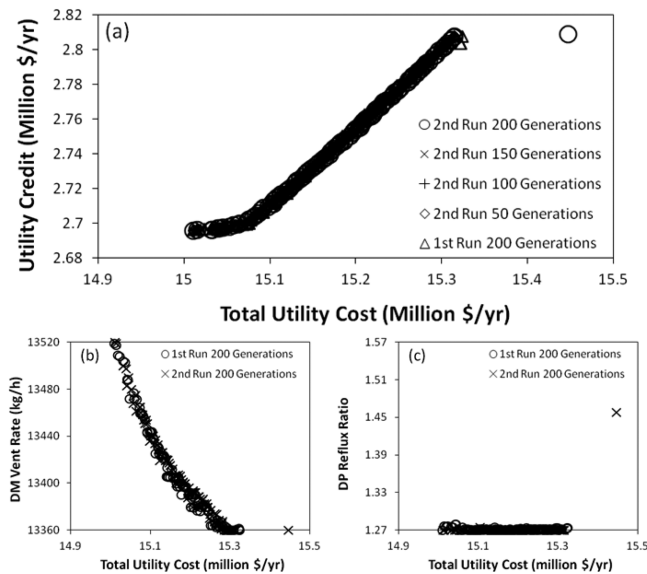


Figure 7. Optimal Pareto front for maximization of utility credit and minimization of total utility cost, at different generations, with only DM vent rate and DP reflux ratio as decision variables (plot a); plots b and c show the optimal values of decision variables corresponding to the Pareto-optimal front from the two runs.

6. CONCLUSIONS

The cold-end separation process in an industrial ethylene plant was simulated using Aspen HYSYS. The elitist nondominated sorting genetic algorithm, NSGA-II implemented in Excel, and Excel-HYSYS interface were then employed for MOO. For validating the HYSYS model, the cold-end separation process was successfully simulated on the basis of design data of an ethylene plant. Operation optimization of this process was then studied for 3 cases of two simultaneous objectives. The Pareto-optimal set for maximizing ethylene production and minimizing net utility cost in the first case was incremental over the range 39 820–39 885 kg/h and 23.0–23.4 million \$/year, respectively. Hence, annual ethylene production can be increased by 0.57 million kg which corresponds to 0.73 million \$/year increase in revenue at the cost of 0.4 million \$/year in utility consumption. The Pareto-optimal front in the second case for maximizing propylene production while minimizing net utility cost increased linearly over the range 14 000–15 400 kg/h of propylene production and net utility cost of 24.2–24.7 million \$/year. For the third case to study the conflicting nature of total utility cost of the process with the utility credit from DM and EF reboilers, the best operating point from the Pareto-optimal front is the one with the lowest utility cost. In all cases, variation of optimal values of decision variables with the objectives can be explained qualitatively, which supports MOO results obtained by NSGA-II. The simulation and optimization methodology of this study can be applied to other schemes of the cold-end separation process of an ethylene plant.

AUTHOR INFORMATION

Corresponding Author

*E-mail: chegpr@nus.edu.sg. Fax: 65 67791936.

Notes

The authors declare no competing financial interest.

REFERENCES

- (1) ICB. *ICIS Chemical Business*, <http://www.icis.com/Articles/2012/11/22/9617145/gpca+ethylene+continues+expansion+in+2012.html>, 2012 (Date of Access: 07-08-2013).
- (2) Bandoni, J. A.; Eliceche, A. M.; Serrani, A.; Debeistegui, R.; Brignole, E. A. Optimal operation of ethylene plants. *Eur. Fed. Chem. Eng., 21st Symp. Comput. Appl. Chem. Eng.*, 1990, 177.
- (3) Petracci, N.; Eliceche, A. M.; Bandoni, A.; Brignole, E. A. Optimal operation of an ethylene plant utility system. *Comput. Chem. Eng.* 1993, 17, S147.
- (4) Eliceche, A. M.; Petracci, N. C.; Hoch, P.; Brignole, E. A. Optimal operation of an ethylene plant at variable feed conditions. *Comput. Chem. Eng.* 1995, 19, 223.
- (5) Petracci, N. C.; Hoch, P. M.; Eliceche, A. M. Flexibility analysis of an ethylene plant. *Comput. Chem. Eng.* 1996, 20, S443.
- (6) Yan, M. *Simulation and Optimization of Ethylene Plant*; Master of Science Thesis, Texas Tech University, 2000, <http://repositories.tdl.org/ttu-ir/bitstream/handle/2346/16119/31295016605676.pdf?sequence=1> (Date of Access: 13-08-2013).
- (7) Sobočan, G.; Glavić, P. Optimization of ethylene process design. *11th European Symposium on Computer Aided Process Engineering 2001*, 9, 529.
- (8) Wang, J.; Smith, R. Synthesis and optimization of low-temperature gas separation processes. *Ind. Eng. Chem. Res.* 2005, 44, 2856.
- (9) Van Geem, K.; Marin, G. B. Computer aided design and optimization of olefin production plants. <http://www.aidic.it/escape20/webpapers/574Marin.pdf>, 2010 (Date of Access: 07-08-2013).
- (10) Zhang, J.; Wen, Y.; Xu, Q. Multiobjective optimization for design and operation of the chilling train system in ethylene plants. *Ind. Eng. Chem. Res.* 2010, 49, 5786.
- (11) Tahouni, N.; Bagheri, N.; Towfighi, J.; Panjeshahi, M. Retrofit of low-temperature gas separation section of an olefin plant. *4th International Conference on Modeling, Simulation and Applied Optimization (ICMSAO) 2011*, 1.
- (12) Tahouni, N.; Panjeshahi, M.; Ataei, A. Comparison of sequential and simultaneous design and optimization in low-temperature liquefaction and gas separation processes. *J. Franklin Inst.* 2011, 348, 1456.
- (13) Masuduzzaman; Rangaiah, G. P. Multi-objective optimization applications in chemical engineering. In *Multi-Objective Optimization: Techniques and Applications in Chemical Engineering*; Rangaiah, G. P., Ed.; World Scientific: Singapore, 2009.
- (14) Sharma, S.; Rangaiah, G. P. Multi-objective optimization applications in chemical engineering. In *Multi-Objective Optimization in Chemical Engineering: Developments and Applications*; Rangaiah, G. P., Bonilla-Petriciolet, A., Eds.; John Wiley: Chichester, U.K., 2013.
- (15) Gao, X.; Chen, B.; He, X.; Qiu, T.; Li, J.; Wang, C.; Zhang, L. Multi-objective optimization for the periodic operation of the naphtha pyrolysis process using a new parallel hybrid algorithm combining NSGA-II with SQP. *Comput. Chem. Eng.* 2011, 32, 2801.
- (16) Li, C.; Zhu, Q.; Geng, Z. Multiobjective particle swarm optimization hybrid algorithm: an application on industrial cracking furnace. *Ind. Eng. Chem. Res.* 2007, 46, 3602.
- (17) Nabavi, S. R.; Rangaiah, G. P.; Niaezi, A.; Salari, D. Multiobjective optimization of an industrial LPG thermal cracker using a first principles model. *Ind. Eng. Chem. Res.* 2009, 48, 9523.
- (18) Nabavi, R.; Rangaiah, G. P.; Niaezi, A.; Salari, D. Design optimization of an LPG thermal cracker for multiple objectives. *Int. J. Chem. React. Eng.* 2011, 9, 1.
- (19) Tarafder, A.; Lee, B. C. S.; Ray, A. K.; Rangaiah, G. P. Multiobjective optimization of an industrial ethylene reactor using a nondominated sorting genetic algorithm. *Ind. Eng. Chem. Res.* 2005, 44, 124.
- (20) Kroschwitz, J. I. *Kirk-Othmer Encyclopedia of Chemical Technology*; John Wiley & Sons: New York, 2004.
- (21) Carlson, E. C. Don't gamble with physical properties for simulations. *Chem. Eng. Prog.* 1996, 35.

- (22) Gmehling, J.; Onken, U.; Arlt, W. *Vapour-Liquid Equilibrium Data Collection*; Chemistry Data Series; Vol.1, Part 6 (a&b), The DECHEMA: Frankfurt am Main, 1980.
- (23) Sinnott, R.; Towler, G. *Chemical Engineering Design*; Butterworth-Heinemann: Oxford, U.K., 2009.
- (24) Kaes, G. *A Practical Guide to Steady State Modeling of Petroleum Processes (Using Commercial Simulators)*, 1st ed.; The Athens Printing Company: Athens, GA, 2000.
- (25) GPSA *Engineering Data Book*; Gas Processors Suppliers Association: Tulsa, OK, 2004.
- (26) Seider, W. D.; Seader, J. D.; Lewin, D. R.; Widagdo, S. *Product and Process Design Principles—Synthesis, Analysis and Evaluation*; John Wiley & Sons: New York, 2010.
- (27) Turton, R.; Bailie, R. C.; Whiting, W. B.; Shaeiwitz, J. A. *Analysis, Synthesis and Design of Chemical Processes*; Pearson Education Inc.: Upper Saddle River, NJ, 2009.
- (28) Sharma, S.; Rangaiah, G. P.; Cheah, K. S. Multi-objective optimization using MS Excel with an application to design of a falling-film evaporator system. *Food Bioprod. Process.* **2012**, *90*, 123.
- (29) Sharma, S.; Lim, Z. C.; Rangaiah, G. P. Process design for economic, environmental and safety objectives with an application to the cumene process. In *Multi-Objective Optimization in Chemical Engineering: Developments and Applications*; Rangaiah, G. P., Bonilla-Petriciolet, A., Eds.; John Wiley: Chichester, U.K., 2013.
- (30) Deb, K. *Multi-Objective Optimization using Evolutionary Algorithms*; John Wiley: New York, 2001.
- (31) Lee, E. S. Q.; Rangaiah, G. P. Optimization of recovery processes for multiple economic and environmental objectives. *Ind. Eng. Chem. Res.* **2009**, *48*, 7662.
- (32) Al-Mayyahi, M. A.; Hoadley, A. F. A.; Rangaiah, G. P. CO₂ emissions targeting for petroleum refinery optimization. In *Multi-Objective Optimization in Chemical Engineering: Developments and Applications*; Rangaiah, G.P., Bonilla-Petriciolet, A., Eds.; John Wiley: Chichester, U.K., 2013.